

Unified Description of Nuclear Stopping in Central Heavy-ion Collision from 10A MeV to 1.2A GeV

G. Q. Zhang,^{1,2} Y. G. Ma *,¹ X. G. Cao,¹ C. L. Zhou,^{1,2} X. Z. Cai,¹ D. Q. Fang,¹ W. D. Tian,¹ and H. W. Wang¹

¹*Shanghai Institute of Applied Physics, Chinese Academy of Sciences, Shanghai 201800, China*

²*Graduate School of the Chinese Academy of Sciences, Beijing 100080, China*

(Dated: June 2, 2021)

The detailed analysis of wide excitation function of nuclear stopping has been studied within a transport model, Isospin-dependent Quantum Molecular Dynamics model (IQMD) and an overall good agreement with the INDRA and FOPI experimental data has been achieved. It is found that mean value of isotropy in central Heavy-Ion Collision (HIC) reaches a minimum near Fermi energy and approaches a maximum around 300 - 400A MeV. This suggests that, in statistical average, the equilibration is far from being reached even in central HIC especially near Fermi energy. A hierarchy in stopping of fragments, which favors heavy fragments to penetrate, provides a robust restriction on the global trend of nuclear stopping and could serve as a probe for nuclear equation of state.

PACS numbers: 25.70.-z, 21.65.Mn

I. INTRODUCTION

The equation of state (EOS) of nuclear matter and its transport mechanisms are the focus of Heavy-ion Collisions (HIC) during the past three decades [1–8]. Before the early 1980s, hydrodynamics approaches based on the local equilibration postulate were provided to extract the EOS information from experimental observables [9]. The discovery of collective flow seems to confirm these approaches and their corresponding equilibration conditions. With the development of microscopic transport theories, it is found that the local equilibration postulate is not indispensable. Actually, near Fermi energy, both statistical and dynamical models which are based on very different, even contradictory mechanisms can predict the same multifragmentation phenomenon [10].

During central HIC process, the nuclear stopping governs most of the dissipated energy and constrains the different reaction mechanisms at different incident energies. It can provide the information on the EOS, nucleon-nucleon (N-N) cross section and the degree of the equilibrium reached in HIC [11–20]. Recently, INDRA and ALADIN Collaborations investigated event-by-event nuclear stopping in central HIC at intermediate energies by 4π multidetector [12]. In the experiment [12], a striking minimal stopping at 40A MeV (Fermi energy) for Xe+Sn system was observed. These experimental results are potential to provide important information about the properties of the nuclear matter and help to find out critical clues for the whole dynamical process during HIC. In previous comparison between experimental results and one isospin-dependent Quantum Molecular Dynamics model (IQMD) simulations [13], a significant difference between them is observed. In the experiment [12], below 70A MeV, they show the experimental data far below the

IQMD simulation results and argued that IQMD model overpredicts nuclear stopping power at low energy. However, before comparing the experimental results quantitatively with that of transport model, two important ingredients should be carefully considered. One is the difference between nucleon phase space (the momentum and positions ensemble of all nucleons) and fragment phase space (the momentum and positions ensemble of all fragments) in IQMD, and the other is the criterion of the centrality in the experiment. After considering these two gradients, we find that the nuclear stopping could be served as a potential probe for determining the nuclear EOS.

This article is organized as following: After introducing some details on IQMD model in Sec.II, two gradients are reconsidered in Sec.III: one is the difference between nucleon phase space and fragment phase space and the other is the impact parameter mixing. Then we compare the simulation results of IQMD with INDRA's experiments near Fermi energy as well as FOPI's at higher energy in Sec.IV. Summary and conclusions are given in Sec.V.

II. ISOSPIN DEPENDENT QUANTUM MOLECULAR DYNAMICS (IQMD) MODEL

The Quantum Molecular Dynamics (QMD) [21] model, is a n-body theory, to predict the behavior of HIC at intermediate energies on an event by event basis. The IQMD [22, 23] model, as inheriting from the QMD model, considers the isospin effects at various aspects: different density distribution for neutron and proton, the asymmetry potential term in mean field, experimental cross-section for nucleon-nucleon ($\sigma_{np} \approx 3\sigma_{pp}, \sigma_{pp} = \sigma_{nn}$) and Pauli-blocking for neutron and proton separately. Just like in QMD, each nucleon wave function is represented

*Corresponding author. E-mail address: ygma@sinap.ac.cn

as a Gaussian form in IQMD, which defined as:

$$\phi_i(\vec{r}, t) = \frac{1}{(2\pi L)^{3/4}} \exp\left[-\frac{(\vec{r} - \vec{r}_i(t))^2}{4L}\right] \exp\left[-\frac{i\vec{r} \cdot \vec{p}_i(t)}{\hbar}\right]. \quad (1)$$

Here L is the width parameter for the Gaussian wave-packet, which is found to be dependent on the size of the reacting system, to constrain the stability of system. We use $L = 2.16 \text{ fm}^2$ for Xe+Sn system. The $\vec{r}_i(t)$ and $\vec{p}_i(t)$ are the position and momentum coordinates of nucleon. Performing variation method, equations of the time evolution of the mean position $\vec{r}_i(t)$ and momentum $\vec{p}_i(t)$ are found to be well known Hamilton equations of motion:

$$\dot{\vec{p}}_i = -\frac{\partial \langle H \rangle}{\partial \vec{r}_i} \quad \text{and} \quad \dot{\vec{r}}_i = \frac{\partial \langle H \rangle}{\partial \vec{p}_i}, \quad (2)$$

where $\langle H \rangle$ is the Hamiltonian of the system. So now the problem is to calculate the Hamiltonian of the system.

After applying the Wigner transformation to the single nucleon wave function, one can get Wigner distribution function to describe a single nucleon density in phase space defined as:

$$f_i(\vec{r}, \vec{p}, t) = \frac{1}{\pi^3 \hbar^3} e^{-(\vec{r} - \vec{r}_i(t))^2 \frac{1}{2L}} e^{-(\vec{p} - \vec{p}_i(t))^2 \frac{2L}{\hbar^2}}, \quad (3)$$

and the total density of the system is the sum over all the nucleons.

Then we can get total Hamiltonian in IQMD model:

$$\langle H \rangle = \langle T \rangle + \langle V \rangle, \quad (4)$$

where the meanfield part is

$$\langle V \rangle = \frac{1}{2} \sum_i \sum_{j \neq i} \int f_i(\vec{r}, \vec{p}, t) V^{ij} f_j(\vec{r}', \vec{p}', t) d\vec{r} d\vec{r}' d\vec{p} d\vec{p}'. \quad (5)$$

In QMD model, the two-body potential interaction contains the Coulomb interaction and the real part of the G-Matrix. The later one can be divided into three parts: the contact Skyrme-type interaction, a finite range Yukawa-potential, and a momentum dependent part. Mathematically, the two-body potential interaction can be written as:

$$\begin{aligned} V^{ij} &= G^{ij} + V_{\text{Coul}}^{ij} \\ &= V_{\text{Skyrme}}^{ij} + V_{\text{Yuk}}^{ij} + V_{\text{mdi}}^{ij} + V_{\text{Coul}}^{ij} \\ &= t_1 \delta(\vec{x}_i - \vec{x}_j) + t_2 \delta(\vec{x}_i - \vec{x}_j) \rho^{\gamma-1}(\vec{x}_i) + \\ &\quad t_3 \frac{\exp\{-|\vec{x}_i - \vec{x}_j|/\mu\}}{|\vec{x}_i - \vec{x}_j|/\mu} + \\ &\quad t_4 \ln^2(1 + t_5(\vec{p}_i - \vec{p}_j)^2) \delta(\vec{x}_i - \vec{x}_j) + \frac{Z_i Z_j e^2}{|\vec{x}_i - \vec{x}_j|}, \end{aligned} \quad (6)$$

where Z is the charge of the baryon, $t_1 \dots t_5$ and μ are the parameters to fit the real part of G-matrix and the properties of nuclei. For IQMD model, one additional part, the symmetry potential V_{sym}^{ij} , is added to take into

account the isospin effects. The total potential in IQMD is then written as:

$$V^{ij} = V_{\text{Skyrme}}^{ij} + V_{\text{Yuk}}^{ij} + V_{\text{mdi}}^{ij} + V_{\text{Coul}}^{ij} + V_{\text{sym}}^{ij}, \quad (7)$$

where the symmetry potential

$$V_{\text{sym}}^{ij} = t_6 \frac{1}{\rho_0} T_{3i} T_{3j} \delta(\vec{r}_i - \vec{r}_j) \quad (8)$$

with $t_6 = 100 \text{ MeV}$ for fitting the Bethe-Weizsäcker mass formula, T_3 is the isospin third projection and ρ_0 is the nuclear saturation density (0.16 fm^{-3}).

We focus on the Skyrme potential, the momentum dependent potential, due to their special connection to nuclear EOS.

One can fulfill the calculation for Skyrme potential and momentum dependent in Eq. 5 by introducing the interaction density,

$$\rho_{\text{int}}^i(\vec{r}_i) = \frac{1}{(4\pi L)^{3/2}} \sum_{j \neq i} e^{-(\vec{r}_i - \vec{r}_j)^2 / (4L)}. \quad (9)$$

The momentum dependent potential, which may be optional in QMD and IQMD, is parameterized with the experimental data, can be written as

$$U_{\text{mdi}} = \delta \cdot \ln^2 \left(\epsilon \cdot (\Delta \vec{p})^2 + 1 \right) \cdot \left(\frac{\rho_{\text{int}}}{\rho_0} \right), \quad (10)$$

where $\delta = 1.57 \text{ MeV}$ and $\epsilon = 500 \text{ (GeV/c)}^{-2}$ are taken from the measured energy dependence of the proton-nucleus optical potential [24] and $\rho_{\text{int}} = \sum \rho_{\text{int}}^i(\vec{r}_i)$.

The Skyrme potential is

$$U_{\text{Sky}} = \alpha \left(\frac{\rho_{\text{int}}}{\rho_0} \right) + \beta \left(\frac{\rho_{\text{int}}}{\rho_0} \right)^\gamma, \quad (11)$$

where α , β and γ are the Skyrme parameters, which connect tightly with the EOS of bulk nuclear matter. After fitting the minimum binding energy and the compressibility at the saturation density, one can get the parameters. The nuclear compressibility, which is the second derivative of the energy at the minimum with respect to the density is expressed as:

$$\kappa = 9\rho^2 \frac{\partial^2}{\partial \rho^2} \left(\frac{E}{A} \right). \quad (12)$$

$\kappa = 200 \text{ MeV}$ means soft EOS, while $\kappa = 380 \text{ MeV}$ is for hard EOS. Please see Table I the Skyrme sets of parameters for different EOS.

The other terms can be also calculated by applying the convolution of the interaction with the Wigner distribution function. After all the potential terms are determined, one can solve the equations of motion of the baryons. For the mesons, only Coulomb force is considered.

For the collisions, IQMD uses the experimental cross-section which tell the isospin effects and nuclear medium

	α (MeV)	β (MeV)	γ	δ (MeV)	ε ($\frac{c^2}{\text{GeV}^2}$)
S	-356	303	1.17	—	—
SM	-390	320	1.14	1.57	500
H	-124	71	2.00	—	—
HM	-130	59	2.09	1.57	500

TABLE I: Parameter sets for the nuclear equation of state used in the QMD model. S and H refer to the soft (compressibility $\kappa = 200$ MeV) and hard equations of state (compressibility $\kappa = 380$ MeV), M refers to the inclusion of momentum dependent interaction. The results are taken from [22]

effect [22]. To consider the fermion property, the Pauli-blocking is also adopted after the collisions.

IQMD treats the many body state explicitly, contains correlation effects to all orders and deals with fragmentation and fluctuation of HICs naturally. To recognize fragments produced in HICs, a simple coalescence rule is used with the criteria $\Delta r = 3.5$ fm and $\Delta p = 300$ MeV/c between two considered nucleons. Thus, nucleons dominated in Fermi motion will be constrained in the fragments.

III. DIFFERENCE BETWEEN NUCLEON PHASE SPACE AND FRAGMENT PHASE SPACE AND IMPACT PARAMETER MIXING

To describe nuclear stopping power, the ratio of transverse to parallel quantities is used in the experiment [12]. One definition is the energy-based isotropy ratio R_E ,

$$R_E = \frac{\sum E_{ti}}{2 \sum E_{li}}, \quad (13)$$

where $E_{ti}(E_{li})$ is the c.m. transverse (parallel) kinetic energy and the sum runs over all products event by event. One can expect $R_E = 1$ for isotropy or full stopping, $R_E < 1$ for partial transparency, and $R_E > 1$ for super stopping. Another definition is R_p ,

$$R_p = \frac{2 \sum |p_{ti}|}{\pi \sum |p_{li}|}, \quad (14)$$

where momenta are used instead of energies. However, they are actually the different forms of physics realization of classical Maxwell distribution assumption.

At low energy, two-body collision between nucleons is suppressed by Pauli-blocking greatly and the mean field governs the HIC process. At freeze-out stage, the motion of a large portion of nucleons is limited in certain fragments, in which Fermi motion dominates over the others. While, at higher energy, two-body collision comes to play the dominant role and most of nucleons suffer violent collisions and get excited to become free. In this case, the fragment phase space tends to get closer to the nucleon phase space. While, in previous IQMD simulation by Liu et al. [13], the nuclear stopping was investigated from nucleon phase space at intermediate energy, where the

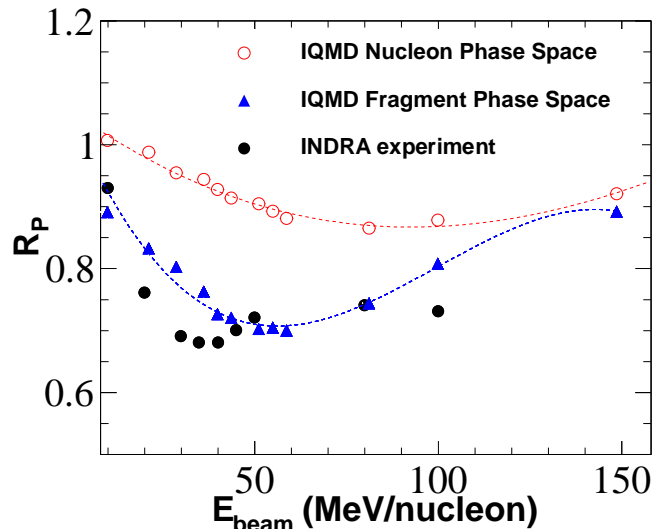


FIG. 1: (Color online) Comparison between experimental stopping values [12] (black points) and predictions of IQMD calculation in nucleon phase space (red open circle) and fragment phase space (blue up triangle) for central $^{129}\text{Xe} + ^{120}\text{Sn}$ collision. Two lines are for guiding the eyes. IQMD adopts the hard EOS and $b_{red} < 0.1$.

isotropic Fermi motion still plays a great role. In comparison with the experimental data of the stopping, the fragment phase space should be applied at intermediate energy within IQMD model rather than nucleon phase space.

In Fig. 1, we show the results of stopping defined as the ratio of transverse momenta to parallel momenta R_p , in nucleon phase space and fragment phase space, respectively. The scaled impact parameter, $b_{red} < 0.1$ ($b_{red} = b/b_{max}$) is adopted, with $b_{max} = 1.12(A_P^{1/3} + A_T^{1/3})$ fm, where A_P and A_T are the mass of projectile and target, respectively. Apparently, stopping calculated in nucleon phase space reaches almost the saturated value, just like Liu's situation [13]. While, in the case of fragment phase space, stopping become far below the saturated value and get closer to the experimental value. It underlies that, at low incident energy, nuclear stopping obtained from fragment phase space is more sensitive as compared to the nucleon phase space and tends to fill the gap between theory and experiments. At higher incident energy (above 100 MeV), the difference between stopping presented in nucleon phase space and fragment space in IQMD, tends to get smaller. However, a minimum stopping with value 0.70 at about 55 MeV is shown in IQMD, compared that with value 0.68 at 40 MeV in experiment. This difference may come from the different criteria of centrality between IQMD and experiment.

To avoid autocorrelations, total charged particle multiplicity (N_{ch}) in the experiment [12] is chosen as the criterion of the centrality. However, the largest N_{ch} does not mean the highest centrality, due to event-by-event fluctuation. On one hand, N_{ch} gets saturated at certain centrality and then central and near central HIC provide similar N_{ch} . On the other hand, due to the dynamical

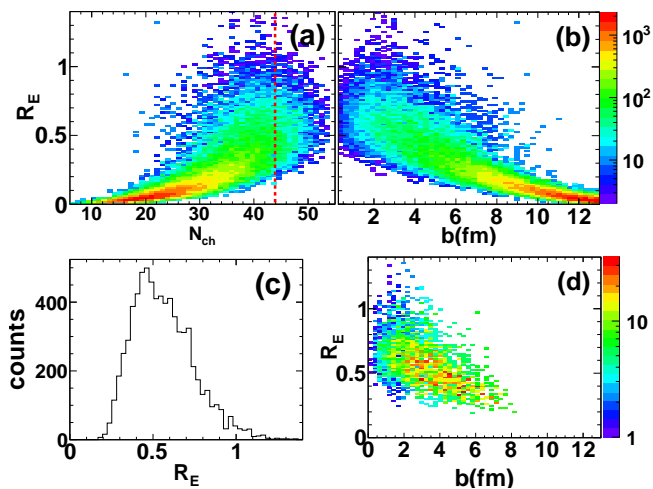


FIG. 2: (Color online) IQMD simulation with the hard EOS for $^{129}\text{Xe} + ^{119}\text{Sn}$ collisions at 50A MeV. (a) Bi-dimensional correlation plot between the mean value of stopping and the total charged particle multiplicity, same as Fig.1(b) in Ref. [12]. (b) Bi-dimensional correlation plot between the mean value of stopping and impact parameter. (c) Distribution of R_E for central collisions. (d) same as (b), but with central collision cut.

fluctuation, N_{ch} at certain centrality presents a broad distribution. Thus, the HIC at different centralities may share the same N_{ch} with a great chance. Hence, if N_{ch} is adopted for the criterion of the centrality, it is expected that the impact parameters will suffer a great mixing and cover a wide range, which will decrease the stopping power and increase the fluctuation of the HIC system greatly.

We now use IQMD model to elucidate the impact parameter mixing situation. In the experiment [12], a typical cross-section of 50 mb for the most total charged particle multiplicity is taken for all HIC systems. Within the IQMD model, we calculate the mean N_{ch} and its width at head-on collision ($b_{red} = 0$). Then, low limit is set as the mean N_{ch} with its half width off. In Fig. 2(a), IQMD model reproduces well the experimental results of INDRA and ALADIN Collaborations [12], except giving a little higher N_{ch} (note that the experimental filter is not used in the present calculation). The red dash line at $N_{ch} = 44$ is the low limit for central collision in IQMD which is comparable with $N_{ch} = 36$ in experiment. In Fig. 2(b), a mean value of stopping (R_E) around 0.6-0.7 is observed in the exact central collision, which has a decreasing trend with the increase of impact parameter. When the cut $N_{ch} = 44$ is applied, there is a broad distribution of impact parameter in Fig. 2(d), and a lower mean value of stopping about 0.56 with a width about 0.42 in Fig. 2(c), which is comparable with that a mean value 0.56 with a width 0.47 in experiment [12]. In this context, better criterion of centrality should be provided to reduce the probability of impact parameter mixing at low energy.

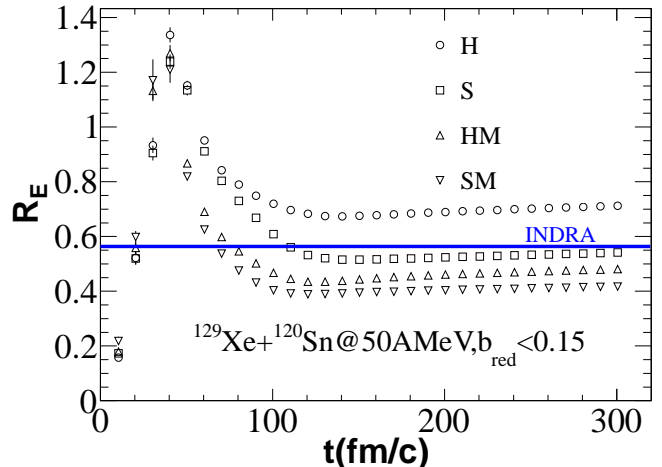


FIG. 3: (Color online) Energy-based stopping values evolution with time for $^{129}\text{Xe} + ^{120}\text{Sn}$ at 50A MeV and $b_{red} < 0.15$ in IQMD (open symbols) and experimental data (solid line) [12]. Circles, squares, up-triangles and down-triangles represent our calculations with the hard (H), the soft (S), the hard with MDI (HM), and the soft with MDI (SM) for EOS, respectively. The horizontal line represents the measured result by the INDRA collaboration (not for the time evolution).

IV. RESTULS AND DISCUSSIONS

Taking the above two key ingredients into account, we can compare the experimental results with those of IQMD quantitatively. To have a broad view of the nuclear stopping, a systematic simulation of $^{129}\text{Xe} + ^{120}\text{Sn}$ is made in very central HIC ($b_{red} < 0.15$) from 10A MeV to 1.2A GeV to cover most of the intermediate energy range, where our results can be compared with the recent INDRA and FOPI data [11, 17].

It should be noted that related but different definitions of stopping are adopted by INDRA [12] and FOPI [11, 17, 19] Collaborations, respectively. The event-by-event stopping (event level) defined as the ratio of transverse to parallel kinetic energies is adopted by INDRA and ALADIN Collaborations (i.e. R_E). While, the ratio of the variances of the transverse to that of longitudinal rapidity distribution of fragment (fragment level) is taken in the case of FOPI experiment

$$vartl = \frac{(\Delta y_t)^2}{(\Delta y_l)^2}. \quad (15)$$

Despite this, they are the same in spirit to show the global stopping power of central HIC. When a full stopping stage (likely to be in equilibration) is reached, both R_E and $vartl$ are required with a value of unit.

Now we compare our results with INDRA experiment. The central ($b_{red} < 0.15$) collision of $^{129}\text{Xe} + ^{120}\text{Sn}$, at incident energy 50A MeV is taken as an example. The time evolution of the stopping (defined in R_E) for various EOS are shown in Fig. 3. The stopping for different EOS presents the same trend. The stopping rises up at the early compression stage, drops down at the following expansion stage and becomes stable after the system

reaches the freeze-out. This is consistent with the results from works of [13] and [14], which are in nucleon phase space. However, the stopping power shows EOS dependence. The hard EOS shows higher stopping than the soft EOS, during the whole time evolution. This is due to the hard EOS nuclear matter is harder to be compressed than the soft one. When compressed from the longitudinal direction, the hard EOS nuclear matter will squeeze out more than the soft one, through the transverse expansion. The momentum dependent force decreases the stopping power of the system, this may result from its repulsive nature and increasing in mean free path [24]. At this incident energy, the INDRA experimental result seems to support the soft EOS.

It may be pointed out that here the time adopted in IQMD for the freeze-out stage is 200fm/c. At low incident energy case, the heavy fragments may still stay at an exciting state, which would deexcite themselves by emitting free nucleons, LCP and gamma rays at the later stage. Basing on this consideration, some hybrid models, a dynamical one followed by a statistical one, come into the play, such as AMD + GEMINI [25–27] and HIPSE + SIMON [28] etc. They do fit the experimental fragment distribution very well. At the same time, the deexcitation procedure may also extend both transverse and longitudinal width of rapidity of the final fragments, which smears the original stopping at fragment level. Especially, the big fragments at high excitation stage will also emit free nucleons or LCPs, which will increase the isotropy of the system. This might be very serious for lower energy ($\leq 40A$ MeV) case due to more heavy fragments are left. As a compensation, the freeze-out time is delayed from 200fm/c to 300fm/c (or even later), but no great changes happen, except for the IMF raise their stopping value a little higher. For higher energy ($\geq 100A$ MeV), since there exists very few heavy fragments, it is not necessary to evolve the system with such a long time or deexcite the system with a statistical process [29].

Fig. 4 shows the excitation function of the mean value of R_E and its width σ_{R_E} for $^{129}\text{Xe} + ^{120}\text{Sn}$ by using different EOS. In Fig. 4(a), the soft EOS with the compressibility of $\kappa = 200$ MeV is taken to show the distribution of R_E with incident energies. In Fig. 4 (b) and (c), the mean R_E and its width σ_{R_E} show the same trends, consistent with the experimental results [12]. Scaled by 0.75, the width of stopping in the experiment of INDRA is compared with the simulation results. The broader widths in experiment could come from the impact parameter mixing, as we have discussed in Sec.II. For all the considered energy range, the hard EOS with $\kappa = 380$ MeV shows stronger stopping than the soft EOS. The EOS with momentum dependent interaction (MDI) [24] tends to decrease the stopping at energy below 500A MeV. While the weight of MDI tends to vanish above 500A MeV. Near the Fermi energy, we also observe a minimum of stopping with its minimal width for all EOS. The EOS with MDI favors more penetration and consumes less energy to reach the minimal stopping. The present experi-

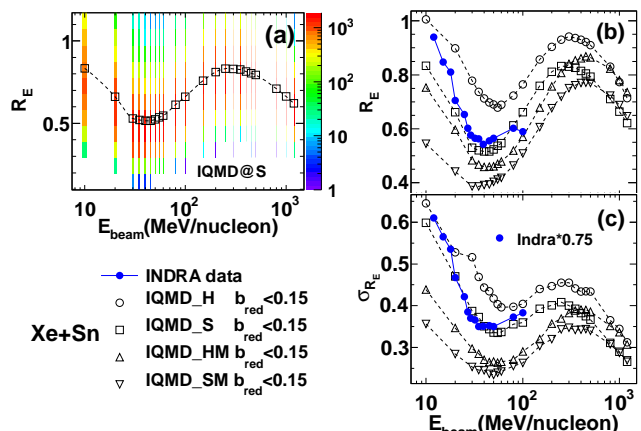


FIG. 4: (Color online) Stopping and its width as a function of incident energy with different EOS for central $^{129}\text{Xe} + ^{120}\text{Sn}$ collision in IQMD (open symbols) and experimental data (solid circles) [12]. (a) Bi-dimensional plots show the distribution of R_E . (b) The mean value of stopping. (c) The width of stopping (Note the widths of experiment have been scaled by a factor 0.75). Circles, squares, up-triangles and down-triangles represent our calculations with the hard (H), the soft (S), the hard with MDI (HM), and the soft with MDI (SM) for EOS, respectively.

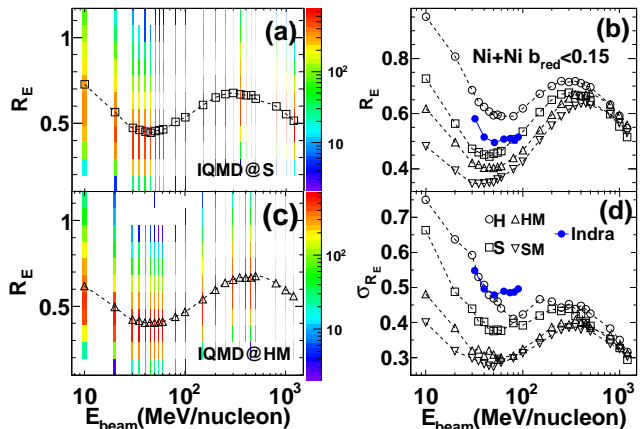


FIG. 5: (Color online) Same as Fig. 4, but for $^{58}\text{Ni} + ^{58}\text{Ni}$ system. One more case (HM), is added in (c) to see the distribution of R_E .

mental results seem to favor the soft EOS around Fermi energy. This also consists with recent conclusion on the soft hadronic matter basing on Kaon spectrum analysis at higher energy [6, 7]. At 300 - 400A MeV, a maximum of stopping accompanied by its maximal width is seen for all EOS. This is comparable to the recent experimental results of FOPI collaboration [11, 17, 19].

The smaller size collision system $^{58}\text{Ni} + ^{58}\text{Ni}$ is also investigated to see the stopping behavior and similar behaviors are found in comparison with the case of $^{129}\text{Xe} + ^{120}\text{Sn}$, except for $^{58}\text{Ni} + ^{58}\text{Ni}$ shows lower stopping power. It may be noticed again, the INDRA data seems to support the soft EOS case. (Fig. 5(b))

Fig. 6(a) displays the atomic number (Z) hierarchy of the degree of stopping at fragment level at different incident energies. From small fragment $Z = 1$ with stopping value 0.7 – 0.9 to intermediate one $Z = 10$ with 0.1 – 0.2,

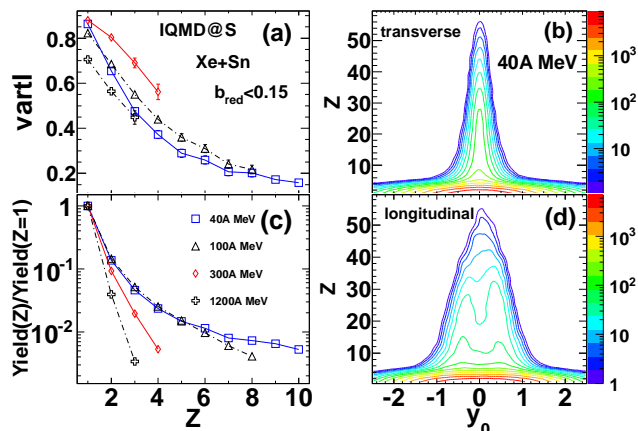


FIG. 6: (Color online) Stopping hierarchy in IQMD with the soft EOS for central $^{129}\text{Xe} + ^{120}\text{Sn}$ collision. Four energy points, namely 40, 100, 300 and 1200A MeV are investigated. (a) and (c) shows Z -dependent stopping at fragment level and the yield of fragments (scaled by $Z=1$), respectively. (b) and (d) displays bi-dimensional distributions of transverse and longitudinal rapidity for different fragments at 40A MeV, respectively.

indicates that the stopping power drops quickly as Z of the fragment increases. Similar trend has been experimentally observed Au + Au, Xe + CsI and Ni + Ni central collisions at 150A MeV, 250A MeV and 400A MeV, by FOPI collaboration [11, 19, 30].

The hierarchies also show the incident energy dependence. On the one hand, at 300A MeV (open diamond in Fig. 6(a)), fragments show stronger stopping than those at the others which is consistent with the maximum event-level stopping at the same energies in Fig. 4. This may suggest a state close to equilibration. On the other hand, at 40A MeV (open square in Fig. 6(a)) where the stopping at event level reaches a minimum (Fig. 4(b)), the stopping at fragment level does show its corresponding smallest value. At this incident energy, most of nucleons are confined in certain fragments, which also reduces the stopping value at event level. Near Fermi energy, the relative yields of intermediate-mass fragments (scaled by $Z = 1$) are higher than those at the others as shown in Fig. 6(c), which will lead to the smallest effective power-law exponents in charge distribution [31]. For a further understanding the minimal stopping near Fermi energy, in Fig. 6(b) and Fig. 6(d), the holographic 2D histogram of transverse and longitudinal rapidity for different charge of fragments are presented (rapidity has been scaled by the projectile rapidity in center of mass system). From $Z = 1$ to larger Z , the longitudinal rapidity distributions become relative broader than the transverse one. In addition, for those fragments with Z larger than about 4, two clear peaks in the longitudinal rapidity stand prominently, corresponding to projectile-like and target-like contribution. This means at Fermi energy, equilibration is far from being reached and entrance channel effects remain strong even in central HIC. While, at high energy 1.2A GeV, fragments are the most transparent.

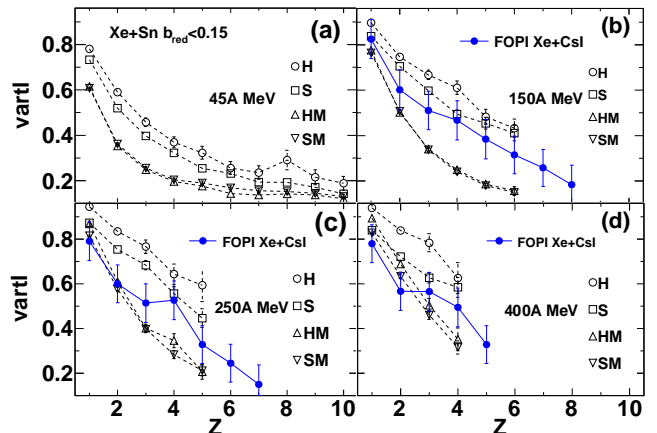


FIG. 7: (Color online) Atomic number dependence of the stopping observable $vartl$ for fragments emitted in central $^{129}\text{Xe} + ^{120}\text{Sn}$ collisions. Open symbols represent our calculations with different EOS and solid symbols with error bar denote the available experimental data [11]. (a) 45A MeV (no experimental data available yet); (b) 150A MeV; (c) 250A MeV; (d) 400A MeV.

It is highly expected that the hierarchy would help to determine nuclear EOS. Fig. 7 shows Z -dependent stopping for four different energies with different EOS in IQMD. The hard EOS case shows higher stopping at fragment level than the soft EOS one, and the MDI always makes it easy for the fragments to penetrate. At lower energy (150A MeV in Fig. 7(b)), the EOS without MDI agrees with FOPI data [11] much better (Xe+CsI are similar system as Xe+Sn). On the contrary, at higher energy (Fig. 7(c) and (d)), to reproduce experimental data, the weight of MDI should be increased. More information could be extracted once more experimental data are provided to low down the statistical fluctuation. In addition, at energy near Fermi energy as shown in Fig. 7(a), it does deserve performing experiment to obtain Z -dependent stopping, which is important to understand the minimal stopping at event level at Fermi energy as well as constrain the EOS.

The atomic number dependence of stopping observable suggests that the heavier fragments have less stopping. This indicates that the heavier fragments are more transparent and keep a stronger entrance channel memory even in the central nuclear collision. This supports the argument that the fragments are not formed in a globally equilibrated environment [21], which contradicts the assumption of equilibrium, required by ideal fluid hydrodynamics. A self-consistent explanation is provided in [19]: if a heavier fragment can survive during the process of HIC, its constituent nucleons should have suffered a less violent collision history. Basing on this consideration, the stopping hierarchy at fragment level would also reflect the N-N cross section. This explanation are also quantitatively demonstrated in earlier version of QMD [32]. Another explanation is due to corona effect (geometrical) [33], even in very central collision, those nucleons near the surface of projectile or target would suffer

less collision history than those inside. Thus, they would keep their original direction and compose the final heavy residues.

In very central HIC, the incident energy dependence of stopping can be understood in a unified structure based on Pauli-blocking, mean field and N-N collision. At intermediate energy, two-body collision between nucleons always increases the dissipation of the HIC system and tends to favor more isotropy. While, Pauli-blocking suppresses N-N collision at low energy, and mean field forms collective motion. This picture shows incident energy dependence. Below Fermi energy, the HIC system has enough time to reach an equilibration state because of the slow process of the reaction. Near Fermi energy, N-N collision is suppressed by Pauli-blocking greatly and nucleons tend to keep their original moving state and have an entrance effect. Meanwhile, mean field dominates HIC, and clusters are then favored. Above Fermi energy, two-body collision between nucleons comes to play the dominant role and reach their maximal effect at 300 - 400A MeV. While, at higher energy, the mean free path of nucleon increases because of the smaller N-N cross section, thus most of nucleons will pass through with each other.

V. SUMMARY AND CONCLUSIONS

In summary, we successfully describe, for the first time, the wide-range excitation function of nuclear stopping

from 10A MeV to 1.2A GeV with a transport model IQMD. A minimum of nuclear stopping value near Fermi energy and a maximum at about 300A MeV in very central HIC match the INDRA and FOPI data very well. The former indicates that in statistical average, equilibration state is far from being reached near Fermi energy even in very central HIC. Meanwhile, the hierarchy of stopping observable together with the yields of fragments, provides us a decomposition way to understand the whole stopping excitation function. Around Fermi energy, the soft EOS seems the best, while at energy from 250 to 400A MeV, the role of MDI becomes important. In addition, it is also highly expected that the isospin which has been regarded to reach its equilibration the fastest at the early HIC process might also get a great penetrating in very central HIC near Fermi energy.

VI. ACKNOWLEDGMENTS

This work is partially supported by the NSFC under contract No.s 11035009, 10979074, 10875160, 10805067 and 10975174, the 973-Program under contract No. 2007CB815004, the Shanghai Development Foundation for Science and Technology under contract No. 09JC1416800, the Knowledge Innovation Project of Chinese Academy of Sciences under Grant No. KJCX2-EW-N01.

-
- [1] P. Danielewicz, R. Lacey and W. G. Lynch, *Science* **298**, 1592 (2002).
 - [2] B. A. Li, L. W. Chen and C. M. Ko, *Phys. Rep.* **464**, 113 (2008).
 - [3] V. Baran et al., *Phys. Rep.* **410**, 335 (2005).
 - [4] M. B. Tsang et al., *Phys. Rev. Lett.* **102**, 122701 (2009).
 - [5] J. B. Natowitz et al., *Phys. Rev. Lett.* **104**, 202501 (2010).
 - [6] C. Hartnack, H. Oeschler and J. Aichelin, *Phys. Rev. Lett.* **96**, 012302 (2006).
 - [7] C. T. Sturm et al., *Phys. Rev. Lett.* **86**, 39 (2001).
 - [8] B. Borderie, M. F. Rivet, *Prog. Part. Nucl. Phys.* **61**, 551 (2008).
 - [9] H. Stöcker et al., *Phys. Rev. Lett.* **47**, 1807 (1981).
 - [10] A. Le Fèvre and J. Aichelin, *Phys. Rev. Lett.* **100**, 042701 (2008).
 - [11] W. Reisdorf et al., *Nucl. Phys. A* **848**, 366 (2010).
 - [12] G. Lehaut et al., *Phys. Rev. Lett.* **104**, 232701 (2010).
 - [13] J.-Y. Liu et al., *Phys. Rev. Lett.* **86**, 975 (2001).
 - [14] X.G. Cao, G.Q. Zhang, X.Z. Cai, Y.G. Ma, W. Guo, J.G. Chen, W.D. Tian, D.Q. Fang, H.W. Wang, *Phys. Rev. C* **81**, 061603(R) (2010).
 - [15] P. Danielewicz et al., *AIP Conf. Proc.* **1128**, 104 (2009).
 - [16] T. Gaitanos et al., *Phys. Lett.* **B595**, 209 (2004).
 - [17] W. Reisdorf et al., *Phys. Rev. Lett.* **92**, 232301 (2004).
 - [18] Y. Zhang, Z. Li, P. Danielewicz, *Phys. Rev.* **C75**, 034615 (2007).
 - [19] A. Andronic et al., *Eur. Phys. J.* **A30**, 31 (2006).
 - [20] S. Kumar, S. Kumar, and R. K. Puri, *Phys. Rev. C* **81**, 014601 (2010).
 - [21] J. Aichelin, *Phys. Rep.* **202**, 233 (1991).
 - [22] C. Hartnack et al., *Eur. Phys. J.* **A1**, 151 (1998).
 - [23] C. Hartnack et al., *Nucl. Phys.* **A495**, 303c (1989).
 - [24] J. Aichelin, A. Rosenhauer, G. Peilert, H. Stoecker, W. Greiner, *Phys. Rev. Lett.* **58**, 1926 (1987).
 - [25] Y. G. Ma, R. Wada, K. Hagel et al., *Phys. Rev.* **C65**, 051602 (2002).
 - [26] Z. Chen et al., *Phys. Rev.* **C81**, 064613 (2010).
 - [27] M. Huang et al., *Phys. Rev.* **C81**, 044620 (2010).
 - [28] D. Lacroix, A. Van Lauwe and D. Durand, *Phys. Rev.* **C69**, 054604 (2004).
 - [29] W. Müller, M. Begemann-Blaich and J. Aichelin, *Phys. Lett. B* **298**, 27 (1993).
 - [30] K. Zbiri et al., *Phys. Rev.* **C75**, 034612 (2007).
 - [31] Y. G. Ma, J. B. Natowitz, R. Wada et al., *Phys. Rev. C* **71**, 054606 (2005).
 - [32] P. B. Gossiaux and J. Aichelin, *Phys. Rev.* **C56**, 2109 (1997).
 - [33] W. Reisdorf, *Nucl. Phys. A* **612**, 493 (1997).